JOURNAL OF GEOPHYSICAL RESEARCH, VOL. 114, F01031, doi:10.1029/2008JF001078, 2009

Instrumental record of debris flow initiation during natural rainfall: Implications for modeling slope stability

David R. Montgomery,[1] Kevin M. Schmidt,[2] William E. Dietrich,[3] and Jim McKean[4]

Received 20 May 2008; revised 24 November 2008; accepted 23 December 2008; published 12 March 2009.

[1] The middle of a hillslope hollow in the Oregon Coast Range failed and mobilized as a debris flow during heavy rainfall in November 1996. Automated pressure transducers recorded high spatial variability of pore water pressure within the area that mobilized as a debris flow, which initiated where local upward flow from bedrock developed into overlying colluvium. Postfailure observations of the bedrock surface exposed in the debris flow scar reveal a strong spatial correspondence between elevated piezometric response and water discharging from bedrock fractures. Measurements of apparent root cohesion on the basal (C_b) and lateral (C_l) scarp demonstrate substantial local variability, with areally weighted values of $C_b = 0.1$ and $C_l = 4.6$ kPa. Using measured soil properties and basal root strength, the widely used infinite slope model, employed assuming slope parallel groundwater flow, provides a poor prediction of hydrologic conditions at failure. In contrast, a model including lateral root strength (but neglecting lateral frictional strength) gave a predicted critical value of relative soil saturation that fell within the range defined by the arithmetic and geometric mean values at the time of failure. The 3-D slope stability model CLARA-W, used with locally observed pore water pressure, predicted small areas with lower factors of safety within the overall slide mass at sites consistent with field observations of where the failure initiated. This highly variable and localized nature of small areas of high pore pressure that can trigger slope failure means, however, that substantial uncertainty appears inevitable for estimating hydrologic conditions within incipient debris flows under natural conditions.

Citation: Montgomery, D. R., K. M. Schmidt, W. E. Dietrich, and J. McKean (2009), Instrumental record of debris flow initiation during natural rainfall: Implications for modeling slope stability, *J. Geophys. Res.*, *114*, F01031, doi:10.1029/2008JF001078.

1. Introduction

[2] Rapidly moving shallow landslides (debris flows) triggered during heavy rainstorms can cause catastrophic damage across large regions [e.g., *Jones*, 1973; *Ellen et al.*, 1988]. Advances in modeling the complexity of debris flow mechanics increased dramatically over the past several decades [e.g., *Iverson*, 1997; *Iverson et al.*, 1997, 2000; *Iverson and Vallance*, 2001], as have relatively simple, spatially explicit models for predicting debris flow hazards [e.g., *Burroughs et al.*, 1985; *Okimura and Ichikawa*, 1985; *Okimura and Nakagawa*, 1988; *Hammond et al.*, 1991; *Sidle*, 1992; *Ellen et al.*, 1993; *Montgomery and Dietrich*, 1994; *Dietrich et al.*, 1995, 2001; *Wu and Sidle*, 1995; *Burton and Bathurst*, 1998; *Montgomery et al.*, 1998, 2000; *Casadei et al.*, 2003]. It remains challenging, however, to predict simultaneously both the timing and location of slope failures that lead to debris flows, and the fundamental relationships and simplifications upon which many models are based have not been tested directly because analyses of observed failures generally have to back calculate hydrologic conditions at failure from either incomplete data or inferences based on qualitative observations.

[3] While a number of three-dimensional (3-D) slope-stability analyses have been developed [e.g., *Hovland*, 1977; *Azzouz et al.*, 1978; *Chen and Chameau*, 1983; *Lovell*, 1984; *Leshchinsky et al.*, 1985; *Hungr*, 1987; *Lam and Fredlund*, 1993; *Okimura*, 1994; *Chen et al.*, 2003], most landslide hazard models employ 1-D limit-equilibrium analyses, such as infinite slope analyses [e.g., Selby 1993], that do not account for shear resistance along the sides of the slide. Consequently, factors of safety may be underestimated and back-calculated shear strengths overestimated using one-dimensional methods [*Stark and Eid*, 1998; *Arellano and Stark*, 2000].

[4] Few direct field observations are available to test theories for the controls on shallow landslide initiation and transformation into debris flows under field conditions. Landslides are difficult to observe as they generally occur in remote areas during rare, large magnitude events. Specific sites of landsliding are difficult to forecast, as fine-scale spatial and temporal variations in precipitation and site

[1]Quaternary Research Center and Department of Earth and Space Sciences, University of Washington, Seattle, Washington, USA.
[2]U.S. Geological Survey, Menlo Park, California, USA.
[3]Department of Earth and Planetary Science, University of California, Berkeley, California, USA.
[4]Rocky Mountain Research Station, Forest Service, U.S. Department of Agriculture, Boise, Idaho, USA.

0148-0227/09/2008JF001078$09.00

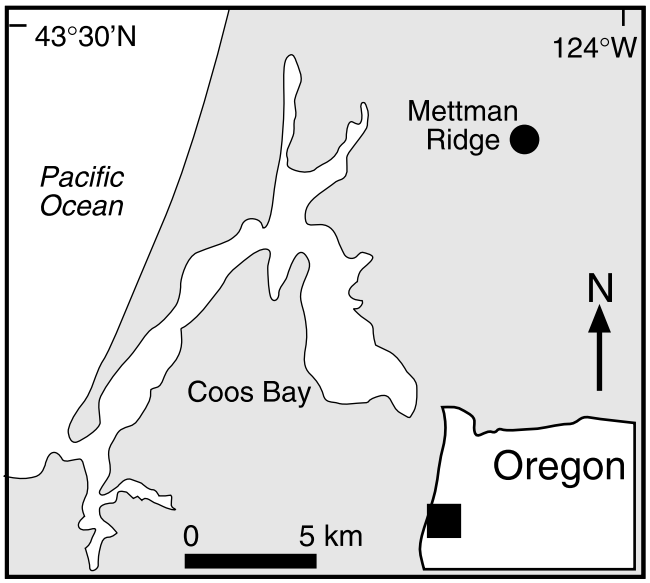

Figure 1. Location map showing position of Mettman Ridge near Coos Bay, Oregon.

properties strongly influence landslide initiation. Several studies have examined the hydrologic conditions associated with debris flow initiation under controlled or manipulated conditions [*Yagi et al.*, 1985; *Yamaguchi et al.*, 1989; *Harp et al.*, 1990; *Reid et al.*, 1997; *Bonte et al.*, 2000; *Iverson et al.*, 2000; *Wang and Sassa*, 2003; *Ochiai et al.*, 2004], and a number of studies have monitored the hydrologic response of landslide-prone hillslopes or slopes where landslides occurred nearby [*Sidle*, 1984; *Wilson and Dietrich*, 1987; *Wieczorek and Sarmiento*, 1988; *Johnson and Sitar*, 1990; *Wilson and Wieczorek*, 1995; *Montgomery et al.*, 1997, 2002; *Fannin and Jaakkola*, 1999; *Onda et al.*, 2001; *Uchida et al.*, 2002, 2003; *Simoni et al.*, 2004; *Matsushi et al.*, 2006]. To date, however, only a few measurements of pore pressure conditions during slope failure under natural conditions exist such as those from a single crest stage piezometer from near the headscarp of a small slide in coastal Alaska [*Sidle and Swanston*, 1982] and discontinuous piezometric records of a slump/debris flow in central California [*Reid et al.*, 1988].

[5] Here we report an instrumental record of slope failure that provides new data on natural debris flow initiation and an opportunity to test models of shallow landslide initiation. We present hydrologic data from the debris flow inducing storm sequence, discuss observations pertaining to the process of debris flow initiation, and evaluate implications for modeling the potential for shallow landsliding.

2. Study Area

[6] The study area is located on Mettman Ridge roughly 15 km north of Coos Bay, Oregon (Figure 1). The Mettman Ridge area consists of steep, highly dissected soil-mantled hillslopes and steep channels typical of the Oregon Coast Range. Landslides are a major geomorphic process in the steep terrain of the Coast Range where hillslope hollows undergo a cycle of slow colluvium accumulation and periodic landsliding [*Dietrich and Dunne*, 1978; *Dietrich et al.*, 1986]. As in many steep landscapes, highly conductive soils and steep slopes focus positive pore pressure development into the axes of topographic hollows [*Pierson*, 1980; *Montgomery et al.*, 1997]. Many channels begin at small landslide scars [*Montgomery and Dietrich*, 1988] and the lower part of hollows may fail more frequently than the upper portions [*Dunne*, 1991; *Montgomery et al.*, 2002]. Intensive timber harvesting and road construction throughout the Oregon Coast Range have dramatically increased rates of landsliding and sediment delivery to downstream channels [e.g., *Brown and Krygier*, 1971; *Beschta*, 1978; *Montgomery et al.*, 2000; *May*, 2002].

[7] The CB1 catchment (Figure 2) on Mettman Ridge is an 860 m^2 source area with an average slope of 43° instrumented for an intensive study of runoff generation, piezometric and tensiometric response, runoff geochemistry, and hollow evolution [*Anderson et al.*, 1997a, 1997b, 2002; *Montgomery et al.*, 1997, 2002; *Torres et al.*, 1998; *Montgomery and Dietrich*, 2002]. CB1 is underlain by gently dipping Eocene sandstone that produces gravelly sandy soil typical of much of the Oregon Coast Range [*Beaulieu and*

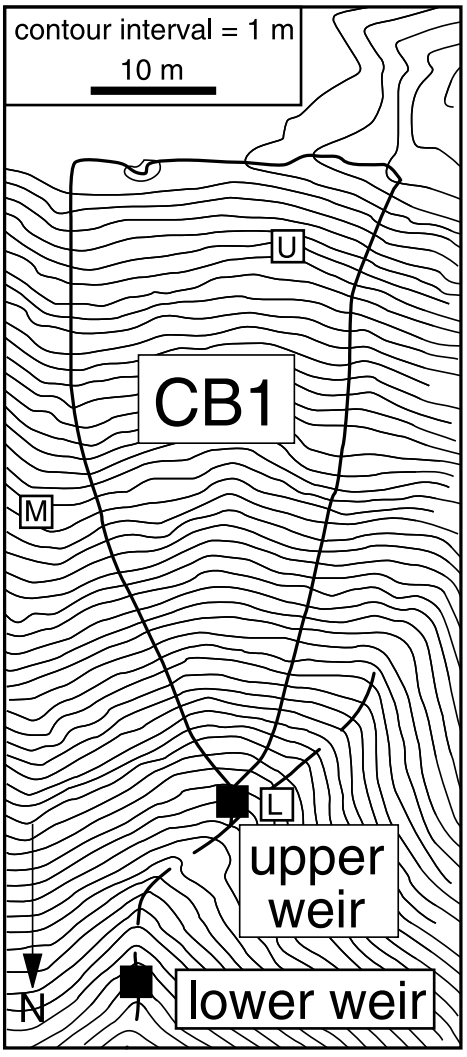

Figure 2. Map of CB1 (outlined polygon) showing position of upper and lower weirs and rain gauge locations (L, CBLOW; M, CBMID; U, CBUPR).

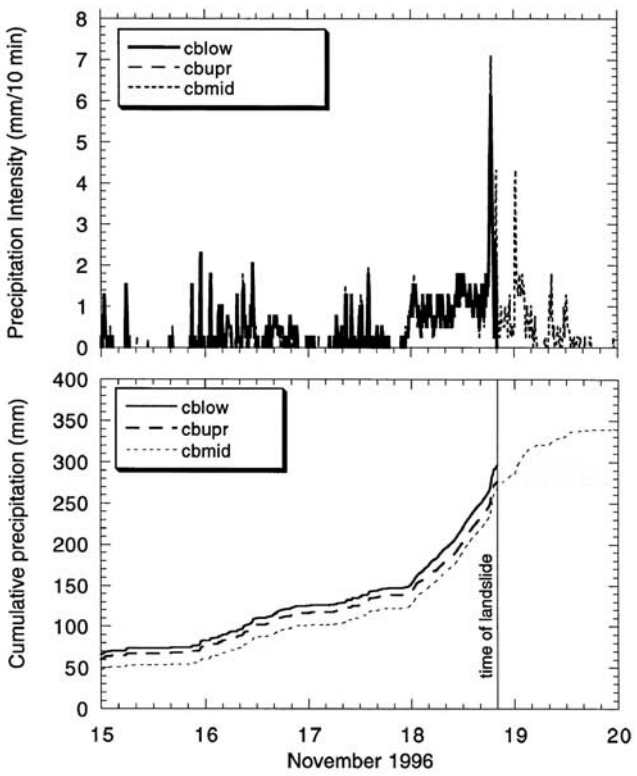

Figure 3. (top) Ten minute intensity and (bottom) cumulative precipitation for 15–20 November 1996 recorded at CB1 (totals include antecedent precipitation starting 12 November). Note termination of CBLOW and CBUPR during passage of the debris flow.

Hughes, 1975; *Haagen*, 1989]. The native *Picea sitchensis* zone forest [*Franklin and Dyrness*, 1988] was clear-cut in 1987, 9 years prior to the landslide/debris flow, and replanted with Douglas fir seedlings in 1988. Annual rainfall averages about 1500 mm, falling mostly during the winter [*Haagen*, 1989].

[8] An extensive piezometer array was installed at CB1 prior to a series of applied rainfall experiments in May 1990 [*Montgomery et al.*, 1997] and expanded to include piezometers installed into bedrock prior to a second set of sprinkler experiments in June 1992. A total of 237 piezometers were installed, 28 of which where installed into bedrock and 42 of which were equipped with pressure transducers. Observations from these experiments and natural storms document that runoff generation occurs by subsurface stormflow mostly through a shallow fractured bedrock zone [*Montgomery et al.*, 2002]. Response of an extensive network of tensiometers showed that during typical rainfall events matric potential (i.e., suction) throughout the soil profile approaches and remains close to zero across the site [*Torres et al.*, 1998] and piezometric data show that a <5 m wide, discontinuous zone of positive pore pressure develops at the base of the soil profile along the hollow axis [*Montgomery et al.*, 1997, 2002]. A seepage face at the channel head generates runoff fed by subsurface flow through near-surface fractured bedrock [*Anderson et al.*, 1997b; *Montgomery and Dietrich*, 2002]. Exfiltrating (i.e., greater than hydrostatic) head gradients develop locally from bedrock into the overlying colluvial soil in response to intense rainfall [*Montgomery et al.*, 1997, 2002]. Two weirs, one installed at the base of CB1 (the upper weir) and the other installed downslope along the colluvial channel (the lower weir), gauged runoff from December 1989 until they were destroyed by a debris flow in November 1996. Fortuitously, fourteen additional single piezometers (i.e., not installed in nests) were installed on the site in October 1996, and were concentrated in the lower half of the site where gaps in the piezometric response had been observed in previous applied rainfall experiments and natural storms [*Montgomery et al.*, 1997, 2002].

[9] In our nomenclature for piezometer nests, each instrument installed in the colluvial soil is labeled by the row number followed by a dash and then the nest number along that row, generally increasing from east to west. Nest 3-1, for example, is the first (i.e., easternmost) nest along row 3. Bedrock piezometers are labeled simply with a prefix of a capital B followed by a nest identification number (e.g., B4). Combined nests of soil and bedrock piezometers are denoted by listing the soil nest first followed by a slash and the associated bedrock piezometer (e.g., 0-1/B4). Lowercase letters after nest identification labels designate individual piezometers, proceeding through the alphabet to identify progressively deeper instruments.

3. November 1996 Storm

[10] A rainstorm from 15–20 November 1996 delivered the largest recorded 24 h rainfall to many areas of the Oregon Coast Range [*Robison et al.*, 1999]. On 18 November a 24 h total of 160 mm of rainfall was recorded at the NOAA/National Weather Service network rain gauge at the North Bend airport, 27 mm greater than the previous daily maximum recorded since 1931. For 16–18 November, the tipping bucket rain gauges at CB1 measured 225 mm of rain with a maximum daily intensity of 145 mm d^{-1} and a 48 h average intensity of 85 mm d^{-1} (Figure 3). These measurements are close to those from the North Bend rain gauge, which recorded a total of 232 mm of rain for the storm and a maximum daily intensity of 169 mm d^{-1}. Rainfall records at two of our CB1 rain gauges terminated at the time of the debris flow because of mechanical disturbance of either the gauge itself or its connection to the data loggers.

[11] During the storm, landslides were widespread in the Oregon Coast Range [*Robison et al.*, 1999], and five lives were lost to debris flows that initiated on steep clear-cut slopes. Five landslides occurred in the 0.43 km^2 area around CB1 during the storm; although the 1996 storm was the storm of record, thirty other landslides had occurred in this area of Mettman Ridge between 1987 and the 1996 storm [*Montgomery et al.*, 2000]. Previous work using a simple coupled hydrologic and digital terrain based slope stability model shows that most landslides in this area occur in locations predicted to have high failure potential [*Montgomery and Dietrich*, 1994; *Montgomery et al.*, 2000; *Dietrich et al.*, 2001], but such models do not explain which of these locations actually fails in particular storms. As is typical, only a portion of the areas predicted topographically to be

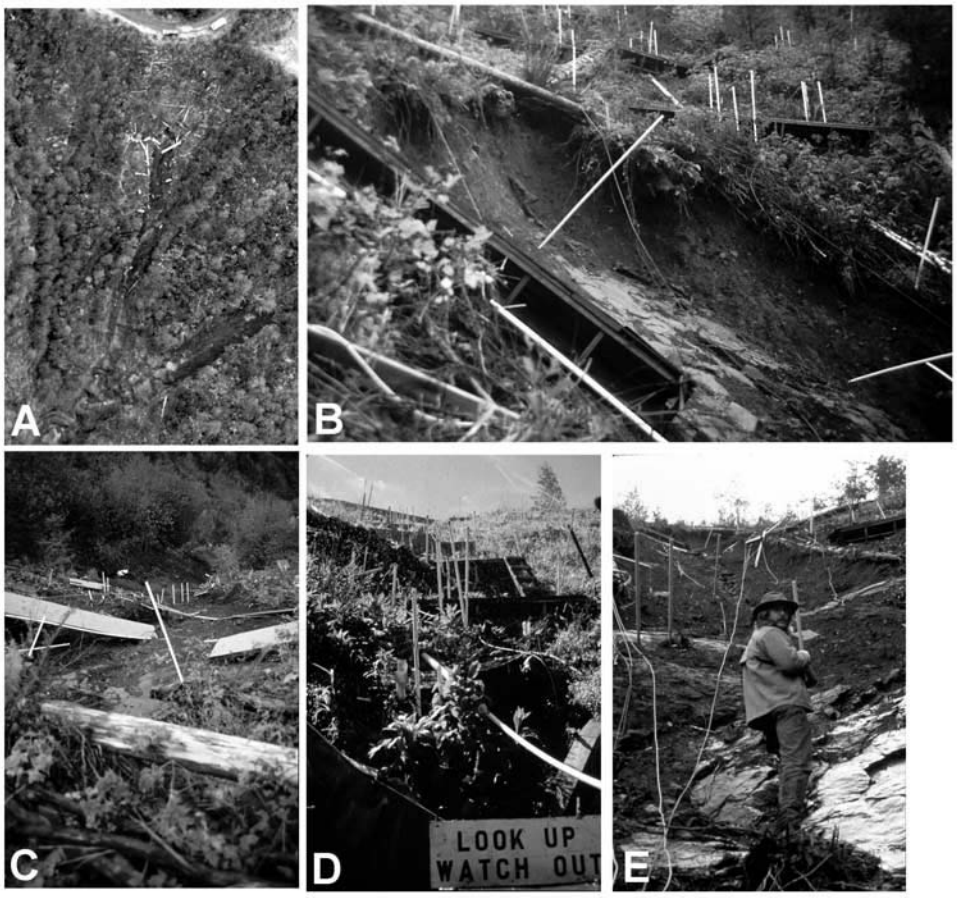

Figure 4. Photographs of CB1. (a) Aerial photograph of CB1 (with broken platforms) and CB2 taken from a low-flying fixed wing aircraft a day after the CB1 landslide and debris flow. Note vehicles parked on ridgetop road for scale. (b) View of landslide headscarp to west from between Rows 6 and 7. (c) View downslope from immediately above the landslide headscarp. (d) View upslope from the base of CB1 at the location of the upper weir during sprinkler experiments in 1992. (e) View upslope the base of CB1 from same location as in Figure 4d taken a day after the CB1 landslide.

least stable along Mettman Ridge failed and generated debris flows in the November 1996 storm [*Montgomery et al.*, 2000].

4. CB1 Debris Flow

[12] One hour after the peak rainfall the slope failed, as recorded by termination of coherent instrument signals for the site. Between 1950 and 2000 local time (LT) on 18 November 1996 colluvium in the hollow in CB1 mobilized as a debris flow, destroying much of the site infrastructure (Figure 4) including the two weirs, a rain gauge, and all but three of the automated piezometer nests (Figure 5). Because of our prior work, we had a detailed topographic map of prefailure conditions that we used to map the failure geometry and record the location of other pertinent observations. Spot elevations surveyed within and around the landslide scar using a total station digital theodolite allowed us to further compare pre- and postfailure conditions. The debris flow left a scar from 0.3 m to about 1 m deep and approximately 5 m wide, extending upslope 26 m (horizontal distance) from the upper weir, which was located at the prefailure channel head.

[13] The debris flow excavated the colluvial soil to the bedrock surface over the upper portion of the scar. Downslope of Row 6 the scoured basal surface was covered with an irregular mantle of colluvium incised by a small gully cut down to bedrock by flow emanating from bedrock fractures at Row 7. Bedrock exposed in the base of the scar was smooth, relatively unfractured sandstone except for three zones in which all of the observed postfailure discharge issued from large fractures. Field observations showed that discharge from CB1 decreased rapidly after the storm, and hand-collected measurements show that CB1 discharge dropped from an estimated 0.6 l s^{-1} at 1400 LT on 22 November to 0.28 l s^{-1} at 1030 LT on 23 November and <0.02 l s^{-1} at 0830 LT on 25 November. The three zones of fractured rock exposed in the floor of the scar correspond to the three zones of partial soil saturation observed in prior sprinkler experiments at CB1 (Figure 6).

[14] Numerous broken roots were exposed on the lateral margins of the landslide scar, and determining the resistance contributed by skin friction or cohesion in tensile failure (as generally assumed in root strength calculations) is a complicated aspect of incorporating different sources of root strength on different slide boundaries in limit equilibrium

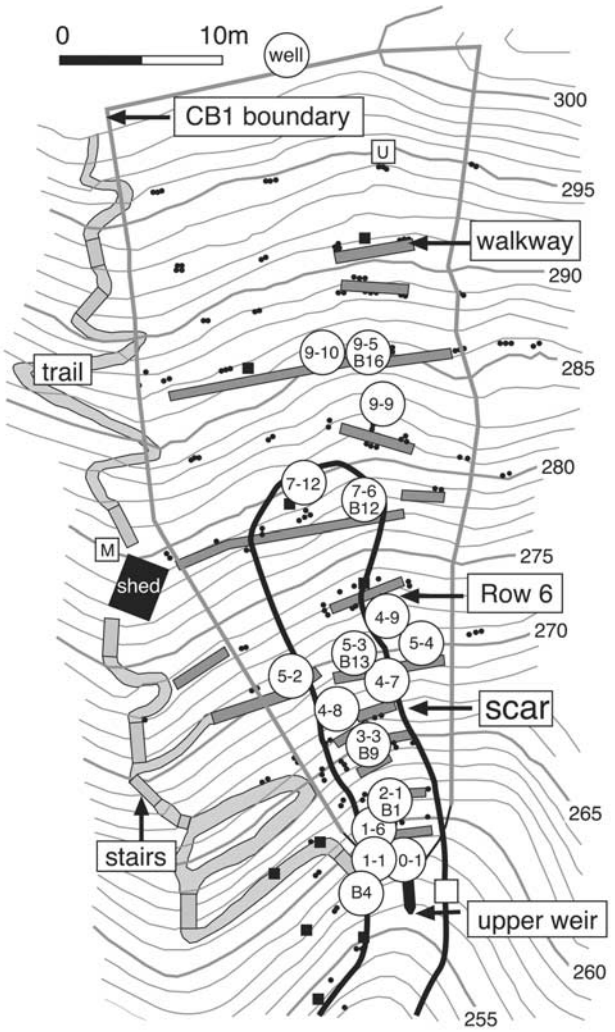

Figure 5. Topographic map of CB1 showing the debris flow scar and location of soil piezometers (small solid circles), bedrock piezometers (small solid squares), automated piezometer nests (large circles shown with piezometer identification labels), automated rain gauges (small open squares; U, CBUPR; M, CBMID; no label, CBLOW), and the upper weir. Thick black line depicts landslide scar; gray polygon denotes CB1 boundary. Contours in meters.

analyses. Although roots exposed in both the headscarp and along the lateral margins of the scarp down to about Row 6 were uniformly snapped, many also protruded into the slide area and hung some distance down the walls of the scar, indicating that either soil flowed out around them, or that they were pulled out of the failing soil as it moved downslope. Broken roots were also exposed in the basal failure surface where the slide occurred above the bedrock surface (i.e., within the colluvial soil). In contrast, some roots exposed on scarp margins downslope of Row 6 were abraded, but retained their entire unbroken dendritic structure, suggesting wear by flowing debris rather than full engagement of their tensile or shear strength during initial failure.

[15] Observations from within the scarp further suggest that the debris flow originated upslope of Row 6 and this mobilized mass traveled across and partially scoured the downslope surface. Upslope of Row 6 colluvium failed down to bedrock, whereas downslope of Row 6 thin patches of the basal colluvial soil remained perched on the bedrock. Between Rows 6 and 7 the debris flow overtopped its scar and 10 to 20 cm of material was deposited on the ground surface, burying vegetation outside of the failure scar downslope to the location of the weir wings at the base of CB1 (Figure 6). Some of the colluvium that overtopped the scar was deposited on top of site infrastructure including catwalks. One intact block of soil, roughly 10 cm in length, was deposited on top of live vegetation such that the block landed upside down with roots exposed at the surface. Trees growing in this depositional area on the margin of the debris flow scar exhibited abrasion marks from 0.28 m to 0.8 m above the ground surface. Wood lying on the edges of the scar (and perhaps the observation platform at Row 6) appeared to have guided the debris flow and resisted deformation as the mobilized material began to sweep downslope.

[16] Piezometers anchored into bedrock were sheared off along the base of the scar between Rows 0 and 5. In contrast, piezometers anchored into bedrock above Row 6 remained standing and, although bent, protruded up into the scar, showing that the colluvial soil flowed out from around the piezometers at the upper end of the scarp. Hence, the debris flow initiated in the upper portions of the resulting scarp and swept downslope entraining material both from the colluvial hollow and the downslope channel.

[17] The CB1 debris flow, together with additional debris flows that originated in the neighboring CB2 catchment (Figure 7) and a bedrock hollow farther downstream (not shown), scoured the downslope channel to bedrock. Surprisingly, roofing tar used to affix the weir wings to the bedrock surface at CB1 remained in place even though the whole weir wing assemblage was stripped to bedrock and an estimated 180 m^3 of colluvial soil was evacuated from upslope and passed over the rock surface to which the tar was affixed. Hence, the debris flow resulted in little to no scour of the bedrock surface at and immediately downslope of the prefailure channel head.

[18] The debris flow traveled almost 1 km downslope, turned an almost right angle at a tributary junction into Sullivan Creek, and scoured another 0.5 km downslope before depositing along a channel reach with an average slope of 1–2% (Figure 7). Debris derived from CB1 infrastructure was distributed along the length of the runout zone, and pieces of the weirs, walkways, and piezometers were recovered from the debris flow deposit. The deposit was composed mostly of matrix-supported debris flow material. In addition, boulders were resting on top of wood incorporated into the deposit, which had a well-defined snout where it came to rest at a lower gradient, wider portion of the valley.

5. Postfailure Analysis of Site Characteristics

[19] After the CB1 landslide, the depth of the landslide scar was measured at locations around the scar perimeter. The average (vertical) depth measured along the perimeter of the landslide scar was 0.7 m. The basal surface was relatively planar with a slope of 43°, parallel to the ground

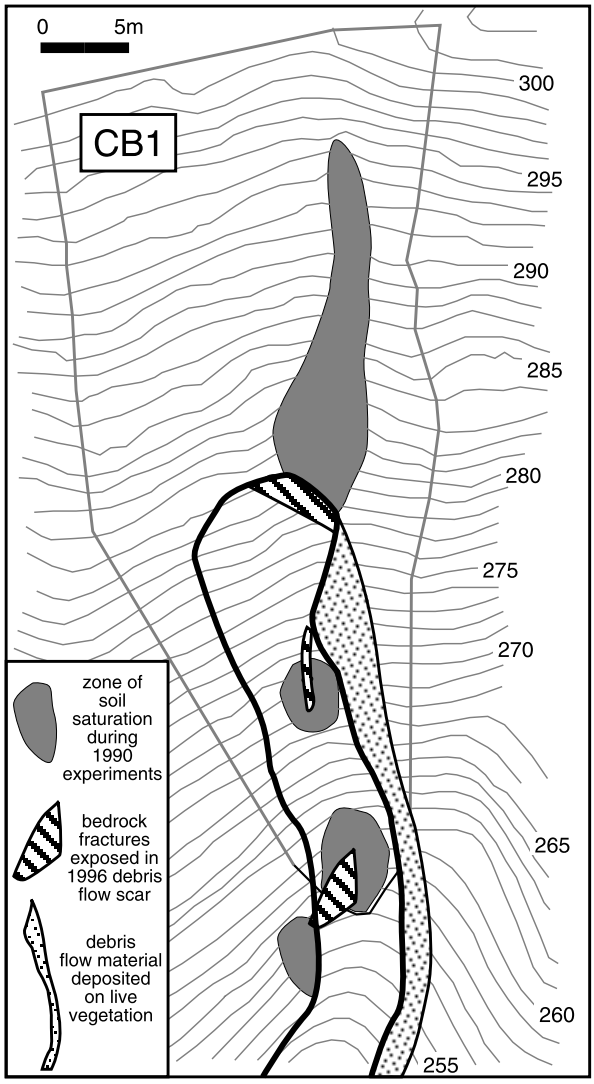

Figure 6. Map of the landslide scar in CB1 showing distribution of fractured bedrock exposed in the base of the failure and the area of the initiation zone in which material flowed over without eroding the original ground surface but instead leaving a thin deposit over live vegetation. Also shown are zones of subsurface saturation that developed during sprinkling experiments reported by *Montgomery et al.* [1997, 2002]. Note that the two zones of saturation at the base of the slope span the weir wings on the upper weir and likely both originate from a fracture zone noted during installation of the weir wings. Contours in meters.

surface. The total basal area of the landslide scar upslope of the CB1 weir was 157 m^2, and the slide perimeter measured 58 m. The total basal area of the landslide scar in the area upslope of Row 6, where it appeared the failure started, was 58 m^2 and the perimeter of the failed area upslope of Row 6 measured 31 m.

[20] Relatively undisturbed samples of the colluvial soil were collected to test soil properties at CB1. We collected samples by vertically inserting 30.5 cm (12″) long × 7.6 cm (3″) wide aluminum Shelby tubes by hand and mallet to minimize disturbance. The mean saturated bulk density of the colluvial soil was 1600 kg m^{-3}; including coarse fragments. Anisotropically consolidated undrained (ACU) triaxial compression strength tests with back pressure saturation and pore pressure measurements were carried out with effective confining stresses intended to mimic in situ stresses within hillslope materials [e.g., *Anderson and Sitar*, 1995]. ACU tests on two samples obtained from CB1 were conducted with effective confining stresses increasing incrementally at three stages for each sample until failure. Effective confining stresses ranged from 9 to 86 kPa for one sample, and from 17 to 97 kPa for the other. Assuming a depth-invariant saturated bulk density of 1600 kg m^{-3}, these stresses are equivalent to a range of approximate soil depths of 0.6–6 m. Envelopes from Mohr circle analyses of triaxial test data on the two samples from Mettman Ridge were determined independently of the specific stress paths. The resulting data for these samples, failing at 5% strain, reveals an effective peak friction angle, φ', of 39.5° and 41° and cohesion, C', of 0 to 1.8 kPa. These values for soil properties at CB1 are comparable to field and laboratory values reported previously for soils developed on sandstone in the Oregon Coast Range [*Yee and Harr*, 1977; *Schroeder*

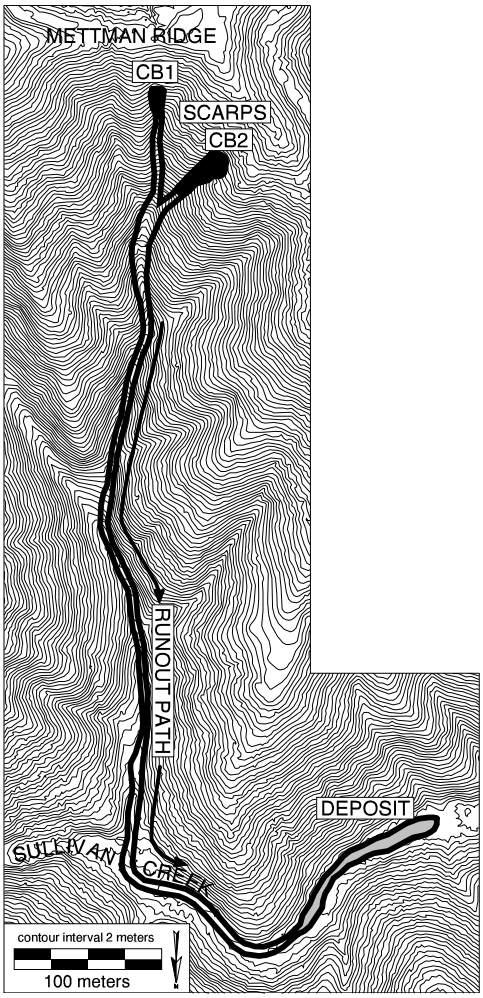

Figure 7. Map of landslides and runout path from laser altimetry showing the location of landslide scarp, debris flow runout path, and deposit. The prefailure channel heads were located at the downslope end of the landslide scarps. Contour interval is 2 m.

and Alto, 1983]. Moreover, as our samples did not have any roots in them, and the laboratory-determined cohesion of 0–1.8 kPa is probably within the margin of error of the tests, the soil (without roots) is virtually cohesionless.

[21] Following procedures described by *Schmidt et al.* [2001], we measured a negligible contribution to shear resistance of an apparent cohesion attributable to roots on the base of the landslide scar (C_b) of 0.1 kPa. In contrast, spatially weighted values for the lateral root cohesion (C_l) exposed in the lateral landslide scarp varied from 0 to 14 kPa for individual segments along the scar perimeter (Figure 8). We obtained a single spatially weighted value representing the lateral root cohesion exposed in the landslide scarp (4.6 kPa) by multiplying the individual segment cohesion values by the ratio of the corresponding segment cross-sectional area relative to the entire cross-sectional area exposed in the scarp perimeter and summed the total. Boundaries of individual segments were chosen to constrain areas of roughly constant cross-sectional area. Alternatively, assuming that each segment cohesion value has equal importance in computing the overall value, we calculate median, arithmetic mean, and geometric mean values of 4.1, 5.0, and 3.0 kPa respectively. The data are not normally distributed and have positive skewness of 1.14. Hence, the geometric mean of 3.0 kPa is likely the most representative central tendency, if all segments are weighted equally. The geometric mean confidence interval (95% confidence level) is calculated to range between 0.83 and 5.2 kPa. For comparison, the spatially weighted value adopted in the slope stability analyses, C_l = 4.6 kPa, falls in the upper range of this mean confidence interval.

[22] To investigate the vertical structure of roots exposed in the landslide scar, we neglected the vertical columns depicted in Figure 8a, and calculated the apparent cohesion attributable to 10 cm depth slices throughout the entire perimeter. Figure 8c reveals a distinct spike in root reinforcement in the 0.1–0.2 m depth interval generally decaying with greater depth in the colluvial deposit. Relations depicted in Figure 8 highlight the assertion that root reinforcement not only varies greatly both laterally and vertically, but also that the highest values are observed well above the median soil depth, consistent with lateral reinforcement outweighing basal reinforcement.

6. Hydrologic Response

[23] The timing of slope failure is recorded by the simultaneous termination of the rainfall records from the rain gauges, the pressure head records from the automated piezometers, and the discharge records from both weirs (Figure 9). Weir wings installed flush with the bedrock surface ensured that discharge through the upper weir recorded flow emerging from the colluvial soil at the channel head. A bypass routed water from both the upper weir, and the hollow immediately west of CB1, past the lower weir, which therefore collected only runoff that entered the channel downslope of the upper weir. Consequently, the upper weir recorded runoff through the colluvial soil from the base of CB1, whereas the lower weir recorded flow emanating from bedrock immediately downslope of the CB1 channel head and direct precipitation on the channel between the weirs. The substantial storm response of the lower weir indicates that the shallow bedrock fracture system is both quite responsive to storm events and accounted for the majority of the runoff from the CB1 catchment during the slide-triggering event.

6.1. Piezometric Response

[24] As found in observations from prior storms and sprinkling experiments at CB1, the response of individual piezometer nests was highly variable in both near-surface bedrock and the overlying colluvial soil (Figure 10). Although most piezometers at CB1 lacked recording pressure transducers, and thus were read by hand during sprinkler experiments, automated records of piezometric response during slope failure are available from five sets of coupled colluvium and bedrock piezometer nests (0-1/B4, 2-1/B1, 3-3/B9, 5-3/B13, 7-6/B12). In addition, data were also available for 14 individual automated piezometers installed approximately one month prior to the landslide. However, seven of these additional piezometers never recorded a signal and therefore were excluded from further analysis because of uncertainty over whether they were functioning properly.

[25] Exfiltrating gradients developed in some piezometer nests, whereas other nests displayed infiltrating gradients throughout the storm. Lowest on the slope, the two piezometer nests closest to the channel head (0-1/B4) showed substantial response in the deepest bedrock piezometer, with total head in the bedrock rising about 0.5 m above the base of the soil (Figure 10a). On 18 November the response in the bedrock was more rapid than in the colluvial soil. By the time that the debris flow initiated, the piezometric gradient had changed from strongly infiltrating to virtually hydrostatic between the bedrock piezometer and those in the colluvial soil. The bedrock piezometer also showed substantial response to rainfall on 16 and 17 November when the response in the colluvial soil was more subdued.

[26] The next piezometer nest upslope from the channel head (2-1/B1) also showed substantial response in the deepest bedrock piezometer (Figure 10b). But in contrast to the nest at the channel head, this nest had exfiltrating gradients throughout the storm, with flow from the shallower bedrock piezometer (B1a) directed upward into the colluvial soil to piezometer 2-1. But even with the exfiltrating gradient, the pore pressure ratio m, defined as the ratio of the pressure head at the base of the soil to the total soil thickness, was substantially less than at the channel head. Nest 3-3/B9, the next nest upslope, displayed infiltrating gradients until the landslide initiated, and had even lower m value, and less relative saturation of the colluvial soil (Figure 10c). The bedrock response at this nest, however, showed a striking (and curious) step-function-like change on 17 November.

[27] Piezometer nest 5-3/B13 showed subdued response in the deepest bedrock piezometer (Figure 10d), but substantial exfiltrating gradients developed from the shallower bedrock piezometer (B13a) into the overlying colluvial soil. Gradients remained infiltrating from the colluvial soil into the underlying fractured rock until 18 November when the total head of B13a exceeded that in both of the two deepest overlying soil piezometers (5-3 and 5-3d). Late in the afternoon of 18 November, over 0.3 m of excess head developed in B13a, but then piezometric gradients dropped

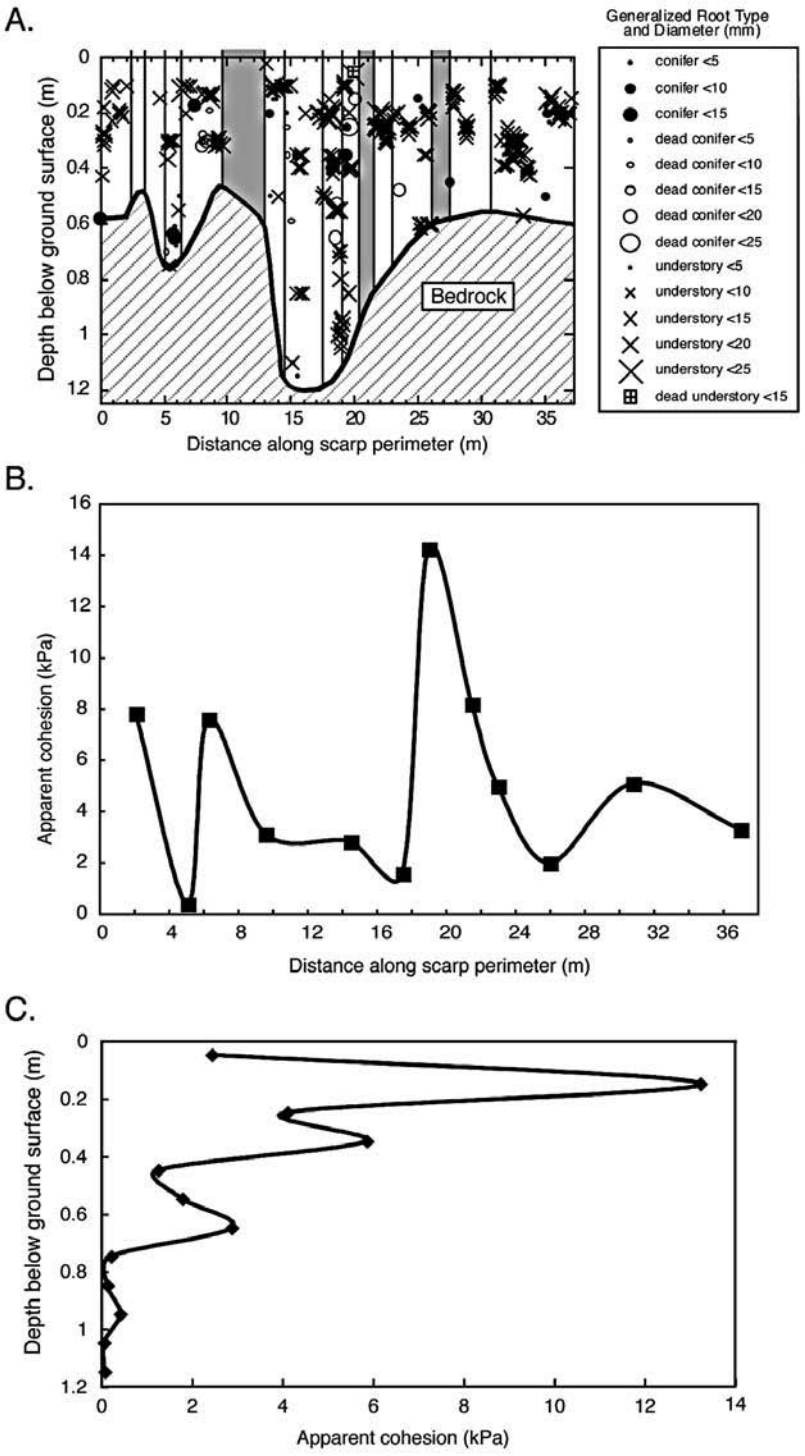

Figure 8. (a) Spatial distribution of root type, size, and depth along the landslide scarp perimeter (running clockwise around the slide from the toe). The net perimeter length shown is shorter than the total perimeter length of 58 m because of disturbance at the ends of the perimeter measurements. Gray-shaded areas are locations where the scar face was disturbed and/or inaccessible. (b) Depth-averaged, spatially weighted apparent cohesion values due to roots along the CB1 landslide perimeter; methods and assumptions are fully described by *Schmidt et al.* [2001]. (c) Apparent cohesion attributable to roots as a function of depth calculated in binned 10 cm thick horizons showing little net reinforcement below 0.8 m.

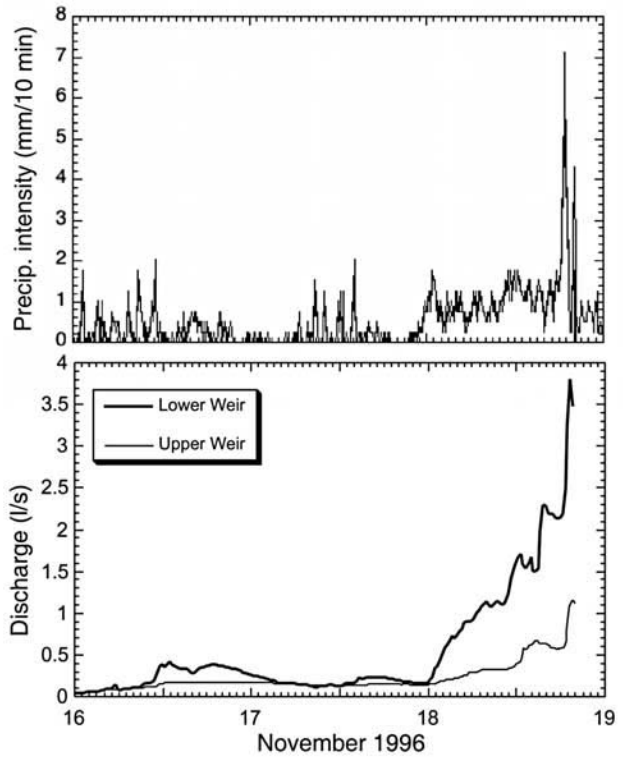

Figure 9. (top) Rainfall intensity and (bottom) discharge from upper and lower CB1 weirs showing termination of the discharge data records initiation of the debris flow.

to hydrostatic immediately prior to debris flow initiation. Hence, at this location, failure occurred about 2 h after peak pressure head in the bedrock (perhaps due to initial soil strain that relieved pore pressure in the underlying rock fractures). Piezometer nest 7-6/B12 had infiltrating gradients until the afternoon of 18 November, when the pore pressure in the deepest bedrock piezometer (B12) rose sharply and developed exfiltrating gradients in the hours immediately prior to initiation of the debris flow (Figure 10e). Throughout, only the lowest portion of the soil was saturated.

[28] The water level in the well at the ridgetop defining the head of CB1 was rising slowly until about noon on 18 November when it began to accelerate. The piezometric level in the well rose 1.5 m in response to the storm and exhibited an approximately 12 h time lag between the change in rainfall intensity and well response. This deep well at the head of the catchment integrates the bedrock response through both near-surface fractured rock and deeper less fractured rock (see well log given by *Anderson et al.* [2002]).

[29] The spatial variability in piezometric response at CB1 during this debris flow-producing storm was similar to that observed in previous storms and sprinkler experiments [*Montgomery et al.*, 1997, 2002]. Within Figure 10, some nests exhibited infiltrating gradients throughout the storm (nests 0-1/B4 and 3-3/B9), whereas others developed exfiltrating gradients indicative of upward flow from bedrock into the soil (nests 2-1/B1, 5-3/B13, and 7-6/B12). Although the magnitude of response was much greater during the November 1996 storm, the style of response and flow paths were similar to those of previous storms and sprinkler experiments. In particular, the spatial pattern of infiltration and exfiltration corresponded with local bedrock fracturing. Flow directions cannot be evaluated for the additional automated piezometers installed individually (i.e., not in a nest) in October 1996.

[30] At the time of landslide initiation, the pore pressure ratio m was quite variable (Figure 11). Within the scar caused by the debris flow, m varied from 0.03 to 0.75 within the length span of roughly 11 m. The data set is small (n = 10), and it is better fit by a lognormal than a normal distribution. Thus, the geometric mean of 0.22 may provide a more appropriate measure than the arithmetic mean of 0.29, and at the 95% confidence level the mean confidence interval is $0.11 > m > 0.42$ for the responsive piezometers within the landslide (i.e., those for which $m > 0$). The automated piezometers located outside of the debris flow recorded m values of 0.01–0.21, with a mean value of 0.12 for the responsive piezometers, about half the mean value for responsive piezometers within the landslide and at the low end of the 95% confidence interval for the geometric mean of values inside the landslide.

[31] The landslide occurred about 1 h after peak runoff through both the upper and lower weirs. At nest 0-1/B4, pressure head in the deepest bedrock piezometer rose until the landslide initiated, whereas head in the two soil piezometers peaked within the hour before the slide. At nest 2-1/B1, head in both bedrock piezometers was rising at the time of failure, although the pore pressure recorded by the soil piezometer had started to drop. At nest 3-3/B9, both the bedrock and soil piezometers were rising at the time of failure. At nest 5-3/B13, the bedrock piezometers peaked 2 h before the slide, and the soil piezometers were still rising at the time of slope failure. Pore pressures in piezometers in both soil and rock at nest 7-6/B12 were rising at the time of the slide. Although the style and magnitude of piezometer response at the time of slope failure was quite variable across CB1, most of the bedrock and soil piezometer nests recorded rising pressure head at the time of failure.

6.2. Evidence of Fracture Flow

[32] As shown in Figure 6, the bedrock exposed in the base of the CB1 landslide scar had three distinct fracture zones; at the uppermost extent of the scar near piezometer nest 7-6/B12, in the middle of the scar at about piezometer nest 5-3/B13, and at the base of CB1 that extended across the original upper weir wings near nest 0-1. The fractures in the lowermost fractured zone were encountered during installation of the weir wings in 1989 and complicated the task of sealing the weir wings to the bedrock surface. Other areas of the bedrock surface exposed in the landslide scar were massive unbroken sandstone with minor siltstone interbeds. Water issuing from the fracture zones was the only active source of runoff from CB1 on the day after the landslide. The flow issuing from the fractures at Row 7 carved a small gully into the colluvium at the base of the failure scar (Figure 4e). All three of the m values greater than 0.4 recorded in the area that failed are from piezometers located at these fracture zones. Hence, the hydrologically active bedrock fracture system at CB1 influenced the

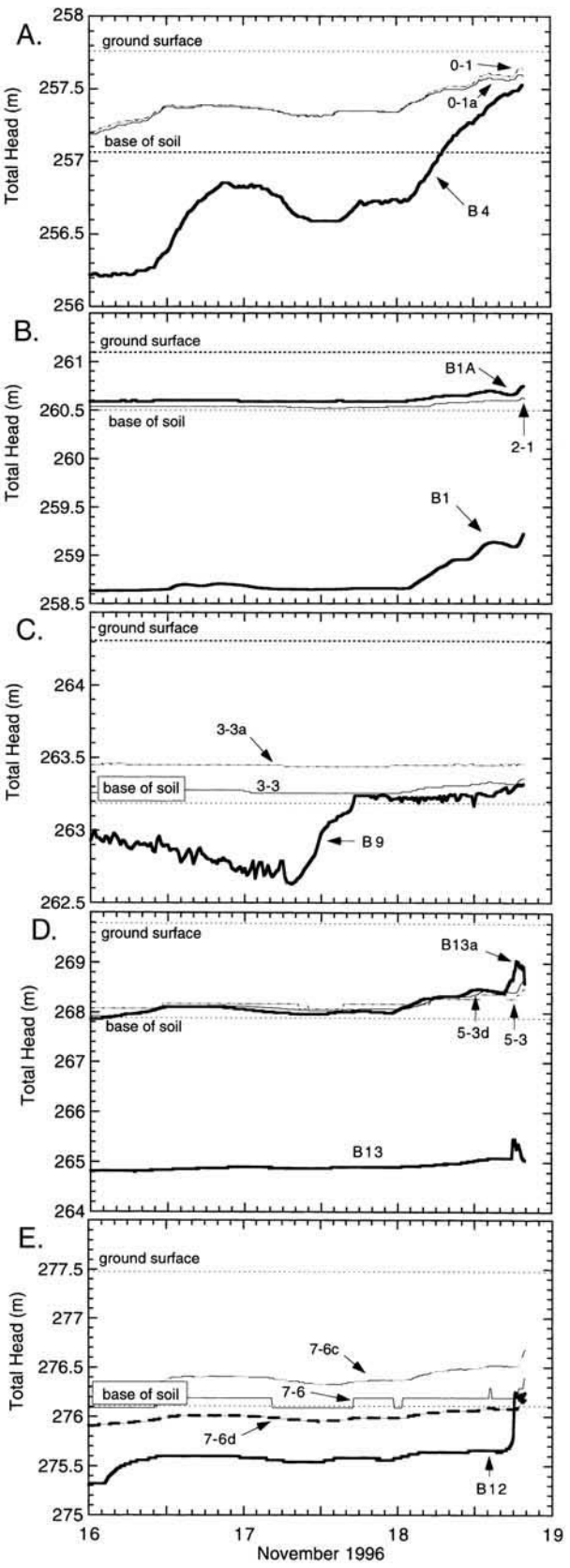

Figure 10. Total head records from 16–19 November 1996 for automated soil and bedrock piezometer nests of (a) 0-1/B4, (b) 2-1/B1, (c) 3-3/B9, (d) 5-3/B13, and (e) 7-6/B12.

spatial variability and maximum values of pore pressure achieved in the overlying colluvial soil, as hypothesized in prior studies both elsewhere [*Wilson and Dietrich*, 1987; *Johnson and Sitar*, 1990; *Mathewson et al.*, 1990; *Anderson and Sitar*, 1995; *Fannin and Jaakkola*, 1999; *Onda et al.*, 2001; *Uchida et al.*, 2002, 2003] and at CB1 [*Montgomery et al.*, 1997, 2002]. Further investigating and/or modeling of how artesian pore pressures propagate through colluvial soil lie beyond the scope of the present study.

7. Model Predictions

[33] In forensic landslide studies, the relative position of the water table at the time of failure generally is not known and therefore must be back calculated. For the CB1 slide,

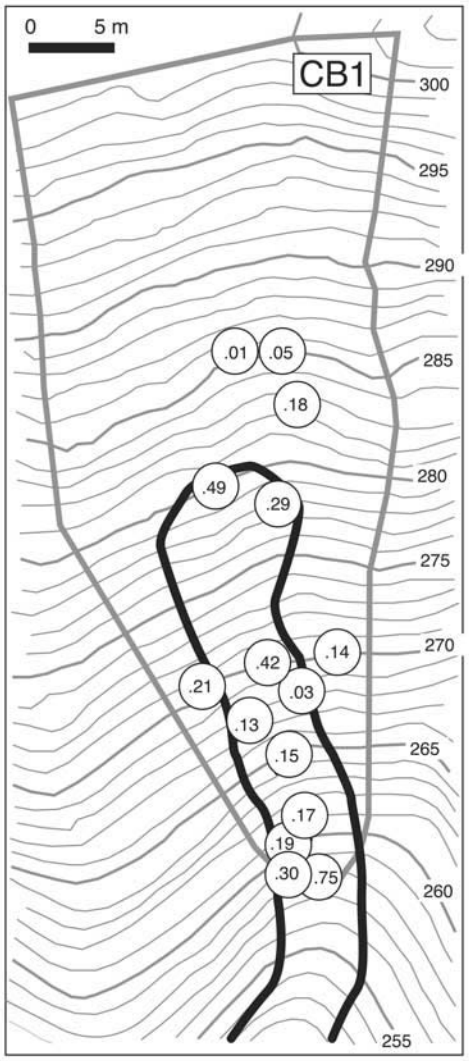

Figure 11. Map of pore pressure ratio; *m* values defined as of the ratio of the pressure head at the base of the soil to the total soil thickness. Shown are values for the automated nests where positive pore pressure response was documented at the base of the soil (we omitted piezometer nest 4-9, which had no response recorded either preceding or during the slide-producing event, and piezometer B4, which is installed into bedrock).

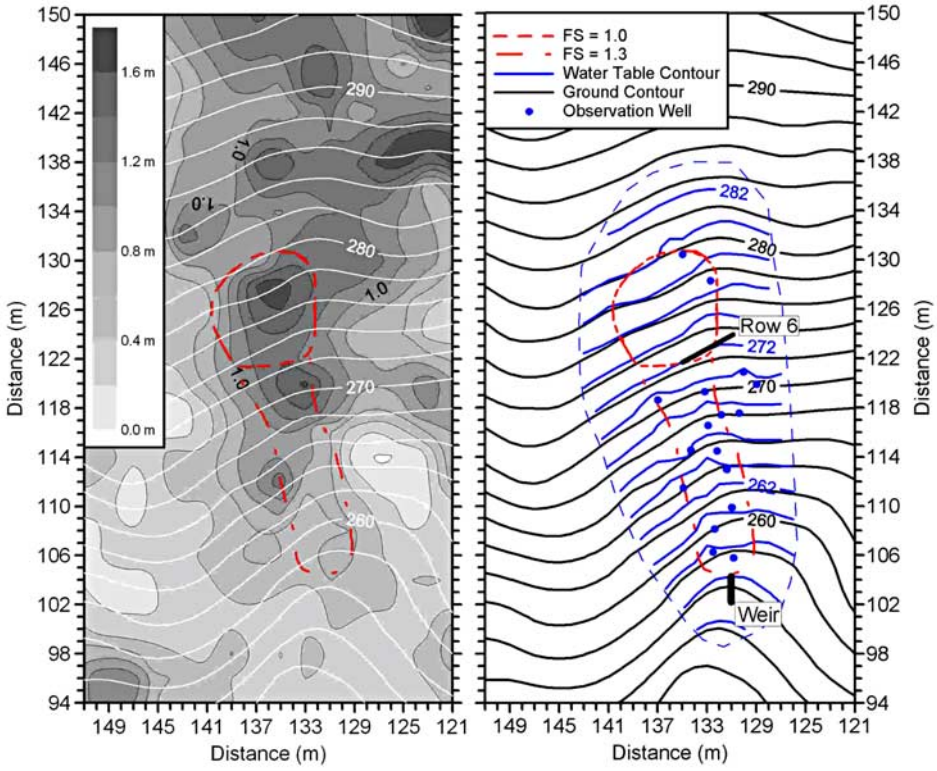

Figure 12. Maps of site conditions and model output from CLARA-W. (left) Spatial pattern of soil thickness (gray scale); topographic contours shown in white. (right) Topography and water table surfaces; black contours are the ground surface, blue contours are the top of the estimated unconfined water table surface, and blue dots are the piezometers upon which the pore pressure field was based. Predicted factors of safety for a failure upslope of Row 6 of the piezometers and a failure of all material in the entire scar upslope of the weir are shown in red. Arbitrary local coordinate system.

however, we can compare measured m values at the time of failure for automated piezometer nests with the critical value calculated as necessary to cause slope failure (m_c) using site-specific characteristics.

[34] In the traditional infinite-slope approximation, flow is often assumed to parallel the failure boundary. In this case, the critical value of the ratio of pore pressure to soil depth required to trigger slope failure may be expressed as

$$m_c = \frac{C + C_r}{\rho_w g z \cos^2\theta \tan\varphi} + (\rho_s/\rho_w)[1 - (\tan\theta/\tan\varphi)], \quad (1)$$

where z is the vertical soil thickness, C is the cohesion of the soil, C_r is the apparent cohesion contributed by plant roots, ρ_s is the saturated bulk density of soil and ρ_w is the density of water, θ is the slope angle, φ is the angle of internal friction of the soil, and g is gravitational acceleration.

[35] Using site-specific values of material properties (C = 0, C_r = 4.6 kPa, z = 0.7 m, φ = 40°, ρ_s = 1600 kg m^{-3}, ρ_w = 1000 kg m^{-3}, and θ = 43°), equation (1) does not yield predictions consistent with observed pore water pressures at the time of slope failure. With C_r = 0.1 kPa (the measured basal root strength, C_b), $m_c = -0.08$, which predicts that the slope should be unstable even if dry (because of $\theta > \varphi$). Hence, the simple one-dimensional, infinite slope model, with pore water pressure predicted from steady groundwater flow parallel to the failure surface, does not perform well at CB1.

[36] The observation that relatively few roots penetrated the basal failure surface, whereas lateral roots were common and broken above Row 6, indicates that a more appropriate model for shallow landslides on vegetated slopes would incorporate the lateral root strength, soil suction in unsaturated soil, and friction along the perimeter of the slide. Building on the approach of previous workers that includes lateral root strength but neglects lateral frictional resistance and soil suction along slide margins [*Riestenberg and Sovonick-Dunford*, 1983; *Reneau and Dietrich*, 1987; *Montgomery et al.*, 2000; *Schmidt et al.*, 2001; *Casadei and Dietrich*, 2003], and again assuming slope parallel flow, the critical degree of soil saturation can be expressed as

$$m_c = \frac{(C + C_b)A + (C + C_l)Pz}{A\rho_w g z \cos^2\theta \tan\varphi} + (\rho_s/\rho_w)[1 - (\tan\theta/\tan\varphi)], \quad (2)$$

where A is the basal area and P is the perimeter of the slide, and C_b and C_l are the apparent cohesion due to roots that cross the basal and lateral surfaces, respectively.

[37] On the basis of field observations from immediately after the CB1 debris flow, we analyzed the following two end-member models of slope failure: (1) initial failure of

only the area upslope of Row 6 and (2) initial failure of the entire scarp upslope of the channel head. Specifically, we analyzed the following two potential slide geometries: (1) the area upslope of Row 6 with an upper width of 9.3 m, a right lateral scarp 7.2 m long, a left lateral scarp 9.9 m long, and a lower width of 4.2 m (perimeter of 31 m and basal area of 58 m^2) and (2) the case of the whole scar upslope of the weir wings with an upper width of 9.3 m, a right lateral scarp 21 m long, a left lateral scarp 23 m long, and a lower width of 5 m (perimeter of 58 m and basal area of 157 m^2).

[38] Using site-specific values of soil properties and slide geometry (as previously but with $C_b = 0.1$ kPa, $C_l = 4.6$ kPa) together with the area and perimeter of just the portion of the slide upslope of Row 6 ($A = 58$ m^2 and $P = 31$ m) yields $m_c = 0.28$. Alternatively, using the area and perimeter of the entire slide ($A = 157$ m^2 and $P = 58$ m) yields $m_c = 0.16$, which predicts the entire slide should have failed before the area upslope of Row 6, contrary to inferences based on our field observations.

[39] The one- and two-dimensional stability methods both treat a landslide as a homogenous rigid block. This assumes that forces applied on the perimeter of a slide act equally throughout the slide body. To better characterize the distribution of forces within as well as on the boundary of the slide, and so more realistically investigate the failure and groundwater conditions at CB1, we used a 3-D version of Spencer's method [*Spencer*, 1967] as implemented in the software CLARA-W (http://www.clara-w.com/ [*Hungr et al.*, 1989]). This technique divides a slope into 3-D cells or columns, and predicts force equilibrium of the collection of columns that describe a slide mass. Some assumptions are required to make the analysis statically determinant. CLARA-W assumes the resultant of shear forces on the sides of the columns acts parallel to the column base. The horizontal shear forces on the lateral sides of a column are assumed equal to the weight of the column multiplied by a constant. This constant is invariant for all columns in a given row across the hillslope, but changes from row-to-row of columns (http://www.clara-w.com/CLW-Manual.pdf). The value of the constant for each row is determined from the force balance of that row and the overall horizontal force balance of the landslide, similar to the approach of *Lam and Fredlund* [1993]. Finally, an assumption is made that the relationship between the vertical shear force and normal force on a column side can be described by a constant "interslice force function," as defined by *Morgenstern and Price* [1965].

[40] The same soil engineering properties were used in the 3-D analysis ($\rho_S = 1600$ kg m^{-3}, a net soil/root cohesion of $C = 4.6$ kPa, and $\varphi = 40°$). An extensive program of soil augering at the CB1 site [*Schmidt*, 1999] closely defined the local pattern of soil depth (see Figure 12 (left)). This allowed a 3-D analysis using columns with an end area of 1×1 m in which the grid system of columns corresponds to the 1 m divisions in the axes of Figure 12 (left). Local soil depth was assigned to each column. To test the influence of column size (as measured by basal area) on predicted overall slide stability, we varied the grid spacing from 0.25 to 2 m. Over this range of grid cell sizes the predicted factor of safety changed by only a few percent for both the area upslope of Row 6 and the whole failure upslope of the upper weir. This variation is well within the range of results caused by uncertainty in local material properties and pore water pressure.

[41] For the 3-D analysis we also relaxed the assumption of groundwater flow parallel to the failure surface and instead estimated a pore pressure field at the time of slope failure from the nonzero recording piezometers. Two of the piezometers that recorded data within or immediately adjacent to the debris flow scar were near the head of the failure and the rest were in the lower portion of the site (below elevation 270 m) where the pressure field was better constrained (Figure 12 (right)). It was necessary to extrapolate from recorded values at the two head scar proximal sites to estimate the pore water pressure pattern in the remainder of the area above Row 6. In the extrapolation we assumed the pore water pressure was unconfined and varied smoothly, albeit rapidly. Using our initial estimate of the pressure field above Row 6, the predicted factor of safety there was 1.05 while it was 1.3 for the entire scar upslope of the weir. With an adjustment of about 10 cm in the estimated pressure head at a few grid nodes in the upper portion of the slide, the predicted factor of safety above Row 6 was 1.0 while the factor of safety of the entire scar upslope of the weir remained 1.3. The unconfined water table contours corresponding to this condition are those shown in Figure 12 (right). Given the pattern of pore water pressure recorded at the base of soil piezometers, the 3-D analysis predicts that failure initiated upslope of Row 6 of the piezometers regardless of the details of our estimate of the full pore pressure field.

8. Discussion

[42] The substantial variability in relative soil saturation within the CB1 landslide at the time of slope failure illustrates the difficulty in evaluating in detail even a simple model for the controls on slope stability (see also *Anderson and Sitar* [1995] and *Dhakal and Sidle* [2004] for related discussion). In particular, the wide range of observed local m values within the area that failed (0.03–0.75) shows that a single value, such as that obtainable from a single piezometer nest, provides a poor representation of the hydrologic condition within an incipient slide mass. This wide range in piezometric response brings up the issue of whether a central tendency or local high values matter more for shallow landslide initiation, as well as how big an area needs to exceed m_c for slope failure to occur. Field observations confirmed that areas where observed m values within the CB1 landslide exceeded the calculated m_c value correspond to locations with exfiltrating flow from bedrock fractures, and our data show that substantial spatial variability in hydrologic response occurs within even a small debris flow.

[43] Although the geometric and arithmetic means of all the m values recorded in the failure zone (0.22 and 0.29) spanned the m_c value predicted by equation (2) (0.28), the wide range in the 95% confidence interval for the geometric mean value (0.11–0.42) indicates that there is substantial uncertainty regarding an m value representative for the incipient landslide as a whole.

[44] All three of the models employed neglect lateral frictional resistance along slide margins. The depth-average frictional shear resistance, S, along simplified vertical boundaries of a slide 0.7 m thick with moist but unsaturated conditions can be roughly estimated from

$$S = K\rho_s g \tan\phi \int_0^{0.7} z dz. \quad (3)$$

Here K is the coefficient of lateral earth pressure. Assuming simple Rankine states of stress and active earth pressure conditions at the head of a slide, at rest pressure on the lateral sides and passive pressure at the boundary on the toe, K is approximated as [*Lamb and Whitman*, 1969]

Headscarp $$K = K_a = \tan^2\left(45 - \frac{\phi}{2}\right) = 0.22,$$

Lateral Boundaries $$K = K_o = 1 - \sin\phi = 0.36,$$

Toe Boundary $$K = K_p = \tan^2\left(45 + \frac{\phi}{2}\right) = 4.60.$$

[45] Using the earth pressure coefficients and material properties reported previously, equation (3) yields lateral frictional strengths of about 1.0, 1.7, and 21.2 kPa respectively, on the head scarp, lateral margins, and toe of the slide. For saturated soils under hydrostatic conditions, equation (3) was modified by reducing the soil bulk density by the density of water. Under such conditions, lateral frictional resistances are estimated to be about 0.4, 0.6, and 7.9 kPa respectively, on the head scarp, lateral margins, and toe of a slide.

[46] Lateral boundary conditions of shallow slides are not well defined and these estimates were made on highly idealized vertical margins. In particular, it is not clear that simple Rankine passive earth pressure conditions are appropriate at the toe boundary. However, this simple analysis does suggest that where there are at rest and active pressure conditions, boundary frictional resistance for saturated conditions on the head and lateral scarps, respectively, are 9 and 13% of the approximated effect of root reinforcement (based on the spatially weighted average lateral root strength measured at the site). Inclusion of lateral soil frictional strength would therefore marginally increase the predicted m_c value at the time of failure. We do not consider the effects of soil suction on slope stability as tensiometers recorded that matric potential (i.e., suction) throughout the soil profile approaches and remains close to zero across the site during rainfall events [*Torres et al.*, 1998].

[47] The 3-D slope stability model CLARA-W predicts that if the upper failure and lower scour zone were treated as a single feature, the soil mass would not have failed. This illustrates both the importance of distinguishing the failure zone from the runout/scoured zone and the difficulty of reconstructing failure conditions based on post-failure morphology.

[48] Development of exfiltrating piezometric gradients from near-surface bedrock into the overlying colluvial soil reflects patterns of bedrock fracturing, which may either enhance or offset spatial patterns of hydrologic response controlled by topographic convergence. The influence of spatial variability in soil thickness, bedrock and soil conductivity, and root strength are all superimposed on a topographically driven hydrological template in steep soil-mantled terrain that is most pronounced on hillslopes with distinct hydrological property contrasts between the bedrock and overlying soil. Consequently, practical hazard predictions need to be based on both observation and understanding of watershed-scale geology and geomorphology and generalities such as expecting slope failures to be more prevalent in topographic hollows than on planar or convex slopes. In this context, the influence of local bedrock fractures on piezometric response in the colluvial soil would explain landslides initiating on planar and convex slopes lacking strong topographic control on hydrologic response.

[49] The data from CB1 present strikingly different response characteristics between piezometers installed into bedrock and colluvium. In all of the nests, the bedrock piezometers showed a larger response and more rapid change. Bedrock piezometers B12, B13, B13a, B9, and B1 all showed rapid, nonlinear rises in pressure head. This nonlinearity may be responsible for quickly raising pore pressures that drive water from the fractured bedrock into a rapidly draining soil matrix, such that localized instability can develop and spread.

[50] The spatial density of information needed to capture the spatial variability of the near-surface hydrologic response of CB1 is daunting. Even with 56 automated piezometers, including eight piezometer nests installed into both bedrock and soil, we recorded an incomplete view of conditions at failure. Indeed, 3-D variably saturated flow simulations from the comprehensive physics-based hydrologic response model Integrated Hydrology Model predict poorly the long-term patterns of dynamic hydrologic response at CB1 [*Ebel et al.*, 2008]. Nonetheless, the spatial variability of hydrologic response documented by the full array of piezometers at CB1 during applied rainfall experiments in 1990 and 1992 [*Montgomery et al.*, 1997, 2002] indicated comparable variability to the near-surface hydrologic response to less intense rainfall. Observations from single piezometers within the slide mass vary across almost the full range of possible m values for the landslide-producing storm. Hence, the reconstruction of failure conditions or interpretation of hazard from small numbers of instruments depends critically on where those instruments are located. This tremendous spatial variability at a scale finer than an individual small landslide shows that substantial uncertainty is inherent in predicting hillslope behavior even when supported by direct instrumental observations.

[51] In addition, our results highlight the problem that soil depths vary over short distances at CB1 and that consequently soil depth is nearly as difficult to parameterize as is the pore pressure field. Much of this variability likely arises from disturbance caused by tree throw and animal burrowing [*Schmidt*, 1999; *Heimsath et al.*, 2001]. Thicker soils also reduce the influence of root strength (equation (2)). Hence, soil depth may be a very strong control on where these local failures initiate, an expectation aligned with the observed propensity for debris flows to initiate in topo-

graphic hollows where colluvial soils progressively thicken [e.g., *Dietrich et al.*, 1995].

[52] The delay between peak rainfall, peak piezometric response, and debris flow initiation in both the 1996 CB1 and the 1992 CB2 events (the latter documented by *Montgomery et al.* [2002]) reflects propagation of the rainfall signal downward through partially saturated soil. The timescale for propagating such a signal into the soil varies with the hydraulic conductivity, soil thickness, the amplitude of the rainfall signal, and the storage coefficient [*Iverson and Major*, 1987; *Haneberg*, 1991]. Because of the greater storm intensity, the time lag of one hour between peak rainfall and debris flow initiation at CB1 during the wetter 1996 storm was much shorter than the 3 to 4.5 h delay for the 1992 CB2 debris flow.

[53] Field observations at CB1 and our analysis confirm that failure of small areas can trigger larger debris flows as they propagate downslope. Lower ratios of pore pressure to soil thickness require larger areas at that m value to trigger failure, indicating that the lateral dimension of zones of elevated pore pressure exerts a primary control on locations and size of slope failure, as argued by *Reneau and Dietrich* [1987], *Gabet and Dunne* [2002], and *Casadei and Dietrich* [2003]. The concentration of near-surface runoff into topographic hollows therefore tends to restrict failures to hollows, except where local hydraulic response leads to small areas of pore pressure high enough to trigger local slope failure in nonconvergent topography. Although not portrayed in topographically driven hazard models, elevated pore pressure sustained over a relatively small area may be sufficient to cause a landslide that could mobilize as a debris flow and scour downslope areas, leaving behind an affected area much larger than the initial slope failure.

9. Conclusions

[54] The observed ratio of pore pressure at the base of the soil to soil thickness varied substantially within the initiation zone of the CB1 debris flow because of patterns of near-surface bedrock fracture flow that superimposed significant local variability on the general topographic control on the convergence of near-surface hydrologic response. Use of measured site properties in the infinite slope model yielded predictions incompatible with field observations, implying that either m or lateral soil resistance (including the effects of lateral friction and apparent cohesion attributable to root strength) must be treated as a calibrated factor in this commonly used model. However, the substantial spatial variability in m values complicates the comparison of critical values calculated from a modified model based on lateral root reinforcement, even though the arithmetic and geometric mean of observed values spanned the predicted critical value. Although the 3-D analysis predicted that failure initiated upslope of Row 6, consistent with field observations, our data document that fine-scale spatial variations in root strength, soil depth, and fracture flow through near-surface bedrock influence the location of individual slope failures, making the prediction of the specific location and timing of failure problematic for practical applications. In particular, our data on hydrologic conditions during debris flow initiation at CB1 show that local variability can overshadow topographic controls on near-surface hydrologic response.

[55] **Acknowledgments.** This project was supported by National Science Foundation grant CMS-9610269. John Buffington, Shannon Hayes, John Heffner, Arjun Heimsath, Maria Panfil, Josh Roering, Jonathan Stock, and Ray Torres provided field assistance immediately after the CB1 debris flow. Tamara Massong, Darryl Granger, and Matt Coglon provided field assistance for topographic surveying. Mark Reid of the U.S. Geological Survey provided the piezometers, installed during October 1996. John Heffner, Jim Clarke, and Kate Sullivan of the Weyerhaeuser Company provided tactical and logistical support for studies at the Coos Bay sites. We also thank Jeff Coe, Ed Harp, Bill Haneberg, and David Milledge for thoughtful comments on draft manuscripts.

References

Anderson, S. A., and N. Sitar (1995), Analysis of rainfall-induced debris flows, *J. Geotech. Eng.*, *121*, 544–552, doi:10.1061/(ASCE)0733-9410(1995)121:7(544).

Anderson, S. P., W. E. Dietrich, R. Torres, D. R. Montgomery, and K. Loague (1997a), Concentration-discharge relationships in runoff from a steep unchanneled catchment, *Water Resour. Res.*, *33*, 211–225, doi:10.1029/96WR02715.

Anderson, S. P., W. E. Dietrich, D. R. Montgomery, R. Torres, M. E. Conrad, and K. Loague (1997b), Subsurface flow paths in a steep unchanneled catchment, *Water Resour. Res.*, *33*, 2637–2653, doi:10.1029/97WR02595.

Anderson, S. P., W. E. Dietrich, and G. H. Brimhall Jr. (2002), Weathering profiles, mass-balance analysis, and rates of solute loss: Linkages between weathering and erosion in a small, steep catchment, *Geol. Soc. Am. Bull.*, *114*, 1143–1158.

Arellano, D., and T. D. Stark (2000), Importance of three-dimensional slope stability analyses in practice, in *Slope Stability 2000*, *Geotech. Spec. Publ.*, vol. 101, edited by D. V. Griffiths, G. A. Fenton, and T. R. Martin, pp. 18–32, GeoInst. of the Am. Soc. of Civ. Eng., Reston, Va.

Azzouz, A. S., M. M. Baligh, and W. Steiner (1978), Three-dimensional slope stability analysis method, *J. Geotech. Eng. Div. Am. Soc. Civ. Eng.*, *104*, 1206–1209.

Beaulieu, J. D., and P. N. Hughes (1975), *Environmental geology of Western Coos and Douglas counties, Oregon*, *Bull. 87*, 148 pp., Oreg. Dep. of Geol. and Miner. Ind., Portland, Oreg.

Beschta, R. L. (1978), Long-term patterns of sediment production following road construction and logging in the Oregon Coast Range, *Water Resour. Res.*, *14*, 1011–1016, doi:10.1029/WR014i006p01011.

Bonte, M., P. Ergenzinger, and A. Rauen (2000), Geomorphological, hydrological and sedimentary control of an artificially induced debris flow, *Phys. Chem. Earth B*, *25*, 745–749.

Brown, G. W., and J. T. Krygier (1971), Clear-cut logging and sediment production in the Oregon Coast Range, *Water Resour. Res.*, *7*, 1189–1198, doi:10.1029/WR007i005p01189.

Burroughs, E. R., Jr., C. J. Hammond, and G. D. Booth (1985), Relative stability estimation for potential debris avalanche sites using field data, paper presented at International Symposium on Erosion, Debris Flow, and Disaster Prevention, Erosion Control Eng. Soc., Tsukuba, Japan.

Burton, A., and J. C. Bathurst (1998), Physically based modelling of shallow landslide sediment yield at a catchment scale, *Environ. Geol.*, *35*, 89–99, doi:10.1007/s002540050296.

Casadei, M., and W. E. Dietrich (2003), Controls on shallow landslide width, in *Debris Flow Hazards Mitigation: Mechanics, Prediction, and Assessment*, edited by D. Rickenmann and C. Chen, pp. 91–102, Millpress, Rotterdam, Netherlands.

Casadei, M., W. E. Dietrich, and N. L. Miller (2003), Testing a model for predicting the timing and location of shallow landslide initiation in soil-mantled landscapes, *Earth Surf. Processes Landforms*, *28*, 925–950, doi:10.1002/esp.470.

Chen, R. H., and J. L. Chameau (1983), Three-dimensional limit equilibrium analysis of slopes, *Geotechnique*, *32*, 31–40.

Chen, Z., H. Mi, F. Zhang, and X. Wang (2003), A simplified method for 3D slope stability analysis, *Can. Geotech. J.*, *40*, 675–683, doi:10.1139/t03-002.

Dhakal, A. M., and R. C. Sidle (2004), Pore water pressure assessment in a forest watershed: Simulations and distributed field measurements related to forest practices, *Water Resour. Res.*, *40*, W02405, doi:10.1029/2003WR002017.

Dietrich, W. E., and T. Dunne (1978), Sediment budget for a small catchment in mountainous terrain, *Z. Geomorphol.*, *29*, 191–206.

Dietrich, W. E., C. J. Wilson, and S. L. Reneau (1986), Hollows, colluvium, and landslides in soil-mantled landscapes, in *Hillslope Processes*, edited by A. D. Abrahams, pp. 361–388, Allen and Unwin, London.

Dietrich, W. E., R. Reiss, M.-L. Hsu, and D. R. Montgomery (1995), A process-based model for colluvial soil depth and shallow landsliding using digital elevation data, *Hydrol. Processes*, *9*, 383–400, doi:10.1002/hyp.3360090311.

Dietrich, W. E., D. Bellugi, and R. R. de Asua (2001), Validation of the shallow landslide model, SHALSTAB, for forest management, in *Land Use and Watersheds: Human Influence on Hydrology and Geomorphology in Urban and Forest Areas*, *Water Sci. Appl. Ser.*, vol. 2, edited by M. Wigmosta and S. Burges, pp. 195–227, AGU, Washington, D. C.

Dunne, T. (1991), Stochastic aspects of the relations between climate, hydrology and landform evolution, *Trans. Jpn. Geomorphol. Union*, *12*, 1–24.

Ebel, B. A., K. Loague, D. R. Montgomery, and W. E. Dietrich (2008), Physics-based continuous simulation of long-term near-surface hydrologic response for the Coos Bay experimental catchment, *Water Resour. Res.*, *44*, W07417, doi:10.1029/2007WR006442.

Ellen, S. D., S. H. Cannon, and S. L. Reneau (1988), Distribution of debris flows in Marin County, in *Landslides, Floods and Marine Effects of the Storm of January 3–5, 1982, in the San Francisco Bay region, California*, *U.S. Geol. Surv. Prof. Pap. Ser.*, vol. 1434, edited by S. D. Ellen and G. F. Wieczorek, pp. 113–131, U.S. Geol. Surv., Reston, Va.

Ellen, S. D., R. K. Mark, S. H. Cannon, and D. L. Knifong (1993), Map of debris flow hazard in the Honolulu District of Oahu, Hawaii, *U.S. Geol. Surv. Open File Rep. 93–213*, 25 pp., Reston, Va.

Fannin, R. J., and J. Jaakkola (1999), Hydrological response of hillslope soils above a debris-slide headscarp, *Can. Geotech. J.*, *36*, 1111–1122, doi:10.1139/cgj-36-6-1111.

Franklin, J. F., and C. T. Dyrness (1988), *Natural Vegetation of Oregon and Washington*, Oreg. State Univ. Press, Corvallis, Oreg.

Gabet, E. J., and T. Dunne (2002), Landslides on coastal sage-scrub and grassland hillslopes in a severe El Niño winter: The effects of vegetation conversion on sediment delivery, *Geol. Soc. Am. Bull.*, *114*, 983–990, doi:10.1130/0016-7606(2002)114<0983:LOCSSA>2.0.CO;2.

Haagen, J. T. (1989), *Soil Survey of Coos County, Oregon*, 269 pp., Natl. Cooper. Soil Surv., Washington, D. C.

Hammond, C., D. Hall, S. Miller, and P. Swetik (1991), Level 1 stability analysis (LISA) documentation for version 2.0, *Gen. Tech. Rep. INT-285*, 190 pp., U.S. Dep. of Agric., Washington, D. C.

Haneberg, W. C. (1991), Pore pressure diffusion and the hydrologic response of nearly saturated, thin landslide deposits to rainfall, *J. Geol.*, *99*, 886–892.

Harp, E. L., W. G. Wells II, and J. G. Sarmiento (1990), Pore pressure response during failure in soils, *Geol. Soc. Am. Bull.*, *102*, 428–438, doi:10.1130/0016-7606(1990)102<0428:PPRDFI>2.3.CO;2.

Heimsath, A. M., W. E. Dietrich, K. Nishiizumi, and R. C. Finkel (2001), Stochastic processes of soil production and transport: Erosion rates, topographic variation and cosmogenic nuclides in the Oregon Coast Range, *Earth Surf. Processes Landforms*, *26*, 531–552, doi:10.1002/esp.209.

Hovland, H. J. (1977), Three-dimensional slope stability analysis method, *J. Geotech. Eng. Div. Am. Soc. Civ. Eng.*, *103*, 971–986.

Hungr, O. (1987), An extension of Bishop's simplified method of slope stability analysis to three dimensions, *Geotechnique*, *37*, 113–117.

Hungr, O., F. M. Salgado, and P. M. Byrne (1989), Evaluation of a three-dimensional method of slope stability analysis, *Can. Geotech. J.*, *26*, 679–686.

Iverson, R. M. (1997), The physics of debris flows, *Rev. Geophys.*, *35*, 245–296, doi:10.1029/97RG00426.

Iverson, R. M., and J. J. Major (1987), Rainfall, ground-water flow, and seasonal movement at Minor Creek landslide, northwestern California: Physical interpretation of empirical relations, *Geol. Soc. Am. Bull.*, *99*, 579–594, doi:10.1130/0016-7606(1987)99<579:RGFASM>2.0.CO;2.

Iverson, R. M., and J. W. Vallance (2001), New views of granular mass flows, *Geology*, *29*, 115–118, doi:10.1130/0091-7613(2001)029<0115:NVOGMF>2.0.CO;2.

Iverson, R. M., M. E. Reid, and R. G. LaHusen (1997), Debris flow mobilization from landslides, *Annu. Rev. Earth Planet. Sci.*, *25*, 85–138, doi:10.1146/annurev.earth.25.1.85.

Iverson, R. M., M. E. Reid, N. R. Iverson, R. G. LaHusen, M. Logan, J. E. Mann, and D. L. Brien (2000), Acute sensitivity of landslide rates to initial soil porosity, *Science*, *290*, 513–516, doi:10.1126/science.290.5491.513.

Johnson, K., and N. Sitar (1990), Hydrologic conditions leading to debris flow initiation, *Can. Geotech. J.*, *27*, 789–801.

Jones, F. O. (1973), Landslides of Rio de Janeiro and the Serra das Araras escarpment, Brazil, *U.S. Geol. Surv. Prof. Pap. 697*, 42 pp., U.S. Geol. Surv., Reston, Va.

Lam, L., and D. G. Fredlund (1993), A general limit equilibrium model for three-dimensional slope stability analysis, *Can. Geotech. J.*, *30*, 905–919, doi:10.1139/t93-089.

Lamb, T. W., and R. V. Whitman (1969), *Soil Mechanics*, 553 pp., John Wiley, New York.

Leshchinsky, D., R. Baker, and M. L. Silver (1985), Three dimensional analysis of slope stability, *Int. J. Numer. Anal. Methods Geomech.*, *9*, 199–223, doi:10.1002/nag.1610090302.

Lovell, C. W. (1984), Three dimensional analysis of landslides, in *Proceedings of the 4th International Symposium on Landslides*, edited by Canadian Geotechnical Society, pp. 451–455, Can. Geotech. Soc., Toronto, Ont., Canada.

Mathewson, C. C., J. R. Keaton, and P. M. Santi (1990), Role of bedrock ground water in the initiation of debris flows and sustained post-flow stream discharge, *Bull. Assoc. Eng. Geol.*, *27*, 73–83.

Matsushi, Y., T. Hattanji, and Y. Matsukura (2006), Mechanisms of shallow landslides on soil-mantled hillslopes with permeable and impermeable bedrocks in the Boso Peninsula, Japan, *Geomorphology*, *76*, 92–108, doi:10.1016/j.geomorph.2005.10.003.

May, C. L. (2002), Debris flows through different forest age classes in the central Oregon Coast Range, *J. Am. Water Resour. Assoc.*, *38*, 1097–1113, doi:10.1111/j.1752-1688.2002.tb05549.x.

Montgomery, D. R., and W. E. Dietrich (1988), Where do channels begin?, *Nature*, *336*, 232–234, doi:10.1038/336232a0.

Montgomery, D. R., and W. E. Dietrich (1994), A physically based model for the topographic control on shallow landsliding, *Water Resour. Res.*, *30*, 1153–1171, doi:10.1029/93WR02979.

Montgomery, D. R., and W. E. Dietrich (2002), Runoff generation in a steep, soil-mantled landscape, *Water Resour. Res.*, *38*(9), 1168, doi:10.1029/2001WR000822.

Montgomery, D. R., W. E. Dietrich, R. Torres, S. P. Anderson, J. T. Heffner, and K. Loague (1997), Piezometric response of a steep unchanneled valley to natural and applied rainfall, *Water Resour. Res.*, *33*, 91–109, doi:10.1029/96WR02985.

Montgomery, D. R., K. Sullivan, and H. M. Greenberg (1998), Regional test of a model for shallow landsliding, *Hydrol. Processes*, *12*, 943–955, doi:10.1002/(SICI)1099-1085(199805)12:6<943::AID-HYP664>3.0.CO;2-Z.

Montgomery, D. R., K. M. Schmidt, H. Greenberg, and W. E. Dietrich (2000), Forest clearing and regional landsliding, *Geology*, *28*, 311–314, doi:10.1130/0091-7613(2000)28<311:FCARL>2.0.CO;2.

Montgomery, D. R., W. E. Dietrich, and J. T. Heffner (2002), Piezometric response in shallow bedrock at CB1: Implications for runoff generation and shallow landsliding, *Water Resour. Res.*, *38*(12), 1274, doi:10.1029/2002WR001429.

Morgenstern, N. R., and V. E. Price (1965), The analysis of the stability of general slip surfaces, *Geotechnique*, *15*, 79–93.

Ochiai, H., Y. Okada, G. Furuya, Y. Okura, T. Matsui, T. Sammori, T. Terajima, and K. Sassa (2004), A fluidized landslide on a natural slope by artificial rainfall, *Landslides*, *1*, 211–219, doi:10.1007/s10346-004-0030-4.

Okimura, T. (1994), Prediction of the shape of a shallow failure on a mountain slope: The three-dimensional multi-planar sliding surface method, *Geomorphology*, *9*, 223–233, doi:10.1016/0169-555X(94)90064-7.

Okimura, T., and R. Ichikawa (1985), A prediction method for surface failures by movements of infiltrated water in a surface soil layer, *Nat. Disaster Sci.*, *7*, 41–51.

Okimura, T., and M. Nakagawa (1988), A method for predicting surface mountain slope failure with a digital landform model, *Shin Sabo*, *41*, 48–56.

Onda, Y., Y. Komatsu, M. Tsujimura, and J. Fujihara (2001), The role of subsurface runoff through bedrock on storm flow generation, *Hydrol. Processes*, *15*, 1693–1706, doi:10.1002/hyp.234.

Pierson, T. C. (1980), Piezometric response to rainstorms in forested hillslope drainage depressions, *N. Z. J. Hydrol.*, *19*, 1–10.

Reid, M. E., H. P. Nielsen, and S. J. Dreiss (1988), Hydrologic factors triggering a shallow hillslope failure, *Bull. Assoc. Eng. Geol.*, *25*, 349–361.

Reid, M. E., R. G. LaHusen, and R. M. Iverson (1997), Debris flow initiation experiments using diverse hydrologic triggers, in *Debris Flow Hazards Mitigation: Mechanics, Prediction, and Assessment*, edited by C.-L. Chen, pp. 1–11, Am. Soc. of Civ. Eng., New York.

Reneau, S. L., and W. E. Dietrich (1987), Size and location of colluvial landslides in a steep forested landscape, in *Erosion and Sedimentation in the Pacific Rim*, *Int. Assoc. Hydrol. Sci. Publ.*, vol. 165, edited by R. L. Beschta et al., pp. 39–49, Int. Assoc. of Hydrol. Sci., Wallingford, U. K.

Riestenberg, M. M., and S. Sovonick-Dunford (1983), The role of woody vegetation in stabilizing slopes in the Cincinnati area, Ohio, *Geol. Soc. Am. Bull.*, *94*, 506–518, doi:10.1130/0016-7606(1983)94<506:TROWVI>2.0.CO;2.

Robison, E. G., K. Mills, J. Paul, L. Dent, and A. Skaugset (1999), Storm impacts and landslides of 1996, *Tech. Rep. 4*, 145 pp., Oreg. Dep. of For., Salem.

Schmidt, K. M. (1999), Root strength, colluvial soil depth, and colluvial transport on landslide-prone hillslopes, Ph.D. thesis, Univ. of Wash., Seattle, Wash.

Schmidt, K. M., J. R. Roering, J. D. Stock, W. E. Dietrich, D. R. Montgomery, and T. Schaub (2001), The variability of root cohesion as an influence on shallow landslide susceptibility in the Oregon Coast Range, *Can. Geotech. J.*, *38*, 995–1024, doi:10.1139/cgj-38-5-995.

Schroeder, W. L., and J. V. Alto (1983), Soil properties for slope stability analysis: Oregon and Washington coastal mountains, *For. Sci.*, *29*, 823–833.

Selby, M. J. (1993), *Hillslope Materials and Processes*, 451 pp., Oxford Univ. Press, Oxford, U.K.

Sidle, R. C. (1984), Shallow groundwater fluctuations in unstable hillslopes of coastal Alaska, *Z. Geltscherkd. Glazialgeol.*, *20*, 79–95.

Sidle, R. C. (1992), A theoretical model of the effects of timber harvesting on slope stability, *Water Resour. Res.*, *28*, 1897–1910, doi:10.1029/92WR00804.

Sidle, R. C., and D. N. Swanston (1982), Analysis of a small debris slide in coastal Alaska, *Can. Geotech. J.*, *19*, 167–174.

Simoni, A., M. Berti, M. Generali, C. Elmi, and M. Ghirotti (2004), Preliminary result from pore pressure monitoring on an unstable clay slope, *Eng. Geol.*, *73*, 117–128, doi:10.1016/j.enggeo.2003.12.004.

Spencer, E. (1967), A method of analysis of the stability of embankments assuming parallel inter-slice forces, *Geotechnique*, *17*, 11–26.

Stark, T. D., and H. T. Eid (1998), Performance of three-dimensional slope stability methods in practice, *J. Geotech. Geoenviron. Eng.*, *124*, 1049–1060, doi:10.1061/(ASCE)1090-0241(1998)124:11(1049).

Torres, R., W. E. Dietrich, D. R. Montgomery, S. P. Anderson, and K. Loague (1998), Unsaturated zone processes and the hydrologic response of a steep unchanneled catchment, *Water Resour. Res.*, *34*, 1865–1879, doi:10.1029/98WR01140.

Uchida, T., K. Kosugi, and T. Mizuyama (2002), Effects of pipe flow and bedrock groundwater on runoff generation in a steep headwater catchment in Ashiu, central Japan, *Water Resour. Res.*, *38*(7), 1119, doi:10.1029/2001WR000261.

Uchida, T., Y. Asano, N. Ohte, and T. Mizuyama (2003), Seepage area and rate of bedrock groundwater discharge at a granitic unchanneled hillslope, *Water Resour. Res.*, *39*(1), 1018, doi:10.1029/2002WR001298.

Wang, G., and K. Sassa (2003), Pore-pressure generation and movement of rainfall-induced landslides: Effects of grains size and fine-particle content, *Eng. Geol.*, *69*, 109–125, doi:10.1016/S0013-7952(02)00268-5.

Wieczorek, G. F., and J. Sarmiento (1988), Rainfall, piezometric levels, and debris flows near La Honda, California, in storms between 1975 and 1983, in *Landslides, Floods and Marine Effects of the Storm of January 3–5, 1982, in the San Francisco Bay Region, California*, *U.S. Geol. Surv. Prof. Pap. Ser.*, vol. 1434, edited by S. D. Ellen and G. F. Wieczorek, pp. 43–62, U.S. Geol. Surv., Reston, Va.

Wilson, C. J., and W. E. Dietrich (1987), The contribution of bedrock groundwater flow to storm runoff and high pore pressure development in hollows, in *Erosion and Sedimentation in the Pacific Rim*, *Int. Assoc. Hyrol. Sci. Publ.*, vol. 165, edited by R. L. Beschta et al., pp. 49–60, Int. Assoc. of Hydrol. Sci., Wallingford, U. K.

Wilson, R. C., and G. F. Wieczorek (1995), Rainfall thresholds for the initiation of debris flows at La Honda, California, *Environ. Eng. Geosci.*, *1*, 11–27.

Wu, W., and R. C. Sidle (1995), A distributed slope stability model for steep forested basins, *Water Resour. Res.*, *31*, 2097–2110, doi:10.1029/95WR01136.

Yagi, N., R. Yatabe, and M. Enoki (1985), Laboratory and field experiments on prediction method of occurring time of slope failure due to rainfall, *Landslide*, *22*(2), 1–7.

Yamaguchi, I., K. Nishio, H. Kawabe, H. Shibano, and C. Iida (1989), Initiation and fluidization of an artificial landslide: Field experiment in Yui Shizuoka Prefecture, Japan (in Japanese), *Shinrin Kosuku*, *158*, 3–9.

Yee, C. S., and R. D. Harr (1977), Influence of soil aggregation on slope stability in the Oregon Coast Ranges, *Environ. Geol.*, *1*, 367–377, doi:10.1007/BF02380505.

W. E. Dietrich, Department of Earth and Planetary Science, University of California, 307 McCone Hall, Berkeley, CA 94720, USA.

J. McKean, Rocky Mountain Research Station, Forest Service, U.S. Department of Agriculture, 322 East Front Street, Suite 401, Boise, ID 83702, USA.

D. R. Montgomery, Quaternary Research Center and Department of Earth and Space Sciences, University of Washington, Box 351310, Seattle, WA 98195, USA. (dave@ess.washington.edu)

K. M. Schmidt, U.S. Geological Survey, 345 Middlefield Road, Mail Stop 973, Menlo Park, CA 94025, USA.